Nano Research
2022, 15(2): 1199–1204
ISSN 1998-0124 CN 11-5974/O4
https://doi.org/10.1007/s12274-021-3625-3

Research Article

Continuous synthesis of ultrasmall core–shell upconversion nanoparticles via a flow chemistry method

Di Liu[§], Junyu Yan[§], Kai Wang (✉), Yundong Wang (✉), and Guangsheng Luo

The State Key Lab of Chemical Engineering, Department of Chemical Engineering, Tsinghua University, Beijing 100084, China
[§] *Di Liu and Junyu Yan contributed equally to this work.*

Received: 14 March 2021 / **Revised:** 19 May 2021 / **Accepted:** 20 May 2021

ABSTRACT

A continuous synthesis method for the less than 10 nm core–shell upconversion nanoparticles was developed via coiled tube embedded flask reactors and a flow solvothermal co-participation reaction up to 300 °C. Fast nucleation of hexagonal nanocrystals in less than 9 min residence time was achieved owing to the excellent heating ability of the reactors, and a two-step reaction strategy was created for the synthesis of β-$NaYF_4$:Gd,Yb,Er/Ho/Tm@$NaYF_4$ particles without intermediate purification.

KEYWORDS

sodium rare earth tetrafluoride, upconversion nanoparticle, core–shell structure, flow chemistry synthesis

1 Introduction

Lanthanide-doped upconversion luminescent nanoparticles (UCNPs) $NaREF_4$, where RE represents the rare earth elements, have unique luminescent properties, which can convert near-infrared (NIR) photons to ultraviolet (UV) or visible (vis) light photons [1]. They have been widely used in the areas of medical imaging [2, 3], bio-detection [4, 5], and targeted drug delivery [6, 7] owing to the strong penetration of NIR through tissues. Among different UCNPs, less than 10 nm and hexagonal formed β-$NaREF_4$ is favored for their excellent biocompatibility and dispersibility [8, 9]. However, these ultrasmall particles suffer from surface quenching problems, strongly influencing their luminescent abilities [10]. Core–shell structured UCNPs are therefore created to eliminate the surface quenching effects [11, 12] and enhance the particle luminescence [13].

Ultrasmall UCNPs are mainly prepared from solvothermal co-precipitation methods [14, 15], which are usually carried out by a high-temperature batch reactor up to 300 °C. The reaction takes 1–3 h to finish the particle nucleation, growth, and crystal form transition from the cubic α-phase to the hexagonal β-phase [16–18]. Although the reaction efficiencies of batch reactors and the batch-to-batch consistency of the particles in those reactors have been fully improved, it still encounters challenges for the mass production of UCNPs. Only limited attempts have been made to synthesize UCNPs on a large scale [19, 20], for example, Wang et al. enhanced the mass transfer of reactants in precursor solution preparation by using high gravity rotating packed bed (RPB) reactors, which intensified the nucleation of particles and ligand distribution on surface. In addition to the improvement of particle precursor, continuous nucleation and growth method of UCNPs is also veiled and highly expected. Currently, flow chemistry methods have been believed to effective methods for the continuous synthesis of nanoparticles such as metals [21], oxides [22, 23], quantum dots [24, 25], perovskites [26, 27], and molecular sieves [28]. However, the synthesis of UCNPs via flow method is rarely reported. The difficulties on the one hand come from the 300 °C high reaction temperature, which has to be well controlled [18, 29]; on the other hand, most synthesis methods require complex intermediate purification for the particles in process, especially for the core–shell UCNPs [30, 31] limiting the reaction continuity. In addition, the causticity of fluoride at high temperature also confines the selection of reactor materials. To overcome these difficulties, coiled tube embedded flask reactors were developed to carry out the solvothermal co-precipitation reaction for β-$NaREF_4$ up to 300 °C in this research, and a two-step reaction without intermediate purification was proposed based on the tubular reactors.

2 Results and discussion

The coiled tube embedded flask reactor is shown in Fig. 1(a). In the flask the coiled tube was used as the flow reactor, whose volume was only 6.5 mL with an inner diameter of 3.7 mm. The flask containing the reaction solvent (60% v/v octadecene (ODE) and 40% v/v oleic acid (HOA)) was heated by an electric heating jacket and it was used as an oil batch to heat the tube. We didn't use other solvent as the heating mediate in this research for the high demand of temperature control in the synthesis of UCNPs, because it has been demonstrated that the mixture of ODE and HOA had excellent temperature controllability in conventional batch experiments. The coiled tube had a strong heat transfer ability, which could heat or cool the inner solution in less than 5 mm distance, as shown by the computational fluid dynamic (CFD) simulation results in Fig. S6 in the Electronic Supplementary Material (ESM). Therefore, the coiled tube embedded flask reactor provided well-controlled heating and cooling processes during the solvothermal co-precipitation reaction. In the experiment, a few bubbles would appear in the

Address correspondence to Kai Wang, kaiwang@tsinghua.edu.cn; Yundong Wang, wangyd@mail.tsinghua.edu.cn

reaction tube, which would help maintain the plug flow in the reactor. Other details of the coiled tube embedded flask reactor and experimental platform are given in the ESM.

In the experiment, β-$NaYF_4$:Gd,Yb,Er were prepared from the precursor solution containing 0.1 M sodium oleate (NaOA), 0.16 M NH_4F, and 0.04 M RE oleate ($RE(OA)_3$) in the mixture of ODE and HOA (RE^{3+} were 50% Y^{3+}, 30% Gd^{3+}, 18% Yb^{3+}, and 2% Er^{3+} in molar percentage, where Y^{3+} was the matrix, Yb^{3+} was the sensitizer, and Er^{3+} was the activator of luminescent light) at first. Gd^{3+} was used in the system according to the researches of Liu et al. [32] and Shi et al. [33], which indicated that Gd^{3+} could promote the crystal transformation from the α-phase to β-phase. Within 45 min in the reactor, the precursor can be successfully converted to β-$NaYF_4$:Gd,Yb,Er as shown in Fig. 1(b). The transmission electron microscope (TEM) images in Fig. 1(c) exhibit uniform β-$NaYF_4$:Gd,Yb,Er particles owning 5–6 nm average diameters from the experiments at 260 and 280 °C. However, the particles were larger and non-uniform from the 300 °C experiment, which indicated the temperature sensitivity of the precipitation reaction. Effects of the precursor flow rate and concentration were also investigated as shown by Figs. S3 and S4 in the ESM. The average particle diameter turned from 6.7 to 4.7 nm, and the diameters was narrowly distributed as increasing the flow rate and shortening the residence time from

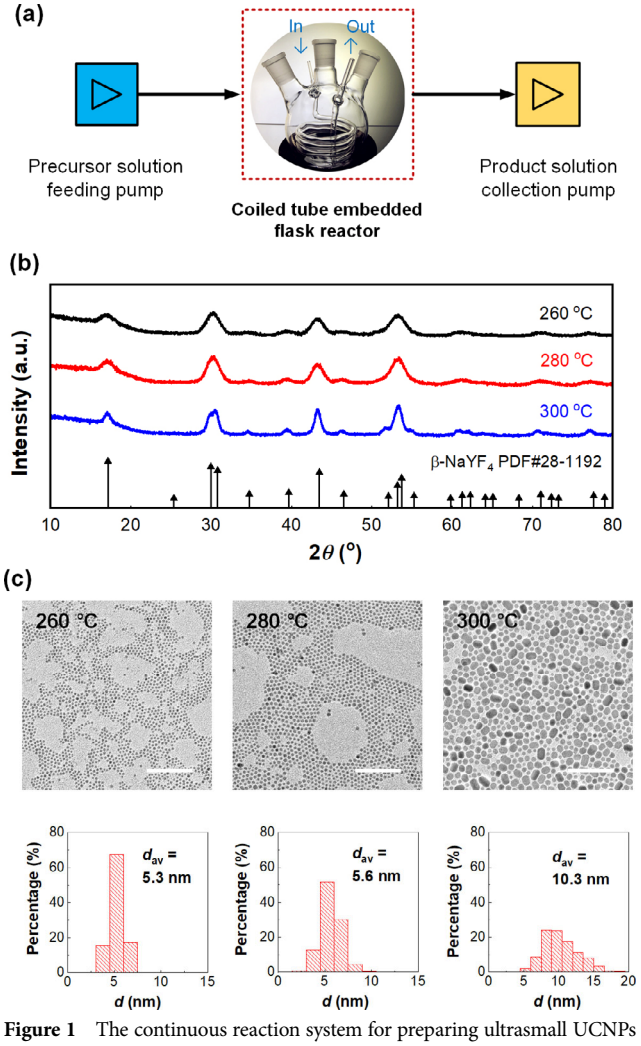

Figure 1 The continuous reaction system for preparing ultrasmall UCNPs and typical results from different temperature experiments. (a) A photo of the coiled tube embedded flask reactor and a schematic of the flow reaction platform. (b) X-ray diffraction (XRD) spectra of β-$NaYF_4$:Gd,Yb,Er from the experiment with the precursor flow rate at 100 μL·min^{-1}. (c) TEM photos of the particles and the diameter statistics. d_{av} is the average diameter. Scale bars show 100 nm.

90 to 30 min, showing the Ostwald-ripening mechanism in the particle growth process. The increase of RE^{3+} concentration from 0.02 to 0.08 M (Na^+, RE^{3+}, and F^- were all increased with a proportion of 2.5:1:4) reduced the particle diameter slightly for enhancing the nucleation by providing more reaction sources. All RE^{3+} conversions that determined by the titration analyses shown in the Methods Section were higher than 97%, owing to strict control of element ratio during the experiments. This important result indicated that very less RE^{3+} was left in the product solution, which avoided the luminescent ions from entering the shells, and helped to omit the purification of particles if we used them as the cores of the core–shell particles.

To in-depth understand the reaction laws, the nucleation of β-$NaYF_4$:Gd,Yb,Er in the coiled tube embedded flask reactor was further investigated. In this experiment, we reduced the reactor inner diameter from 3.7 to 1 mm to shorten the reaction time to 8.5 min at Q = 100 μL·min^{-1}. Because the well mixed precursor solutions (homogenous phase fluid) were used as the reactants and almost the same heating and cooling ability of the thinner reactor as shown by Fig. S6 in the ESM, the reaction environment of this section was almost the same as above. The results in Figs. 2(a) and 2(b) show that β-$NaYF_4$:Gd,Yb,Er appeared from the precursor solution even at 205 °C. The titration results in Fig. 2(c) also show that more than 70% RE^{3+} had been converted in less than 9 min reaction time. Figure 2(b) also shows that NaF was generated at 205 °C for the fast contact of Na^+ and F^-. However, NaF disappeared at 255 °C. At 280 °C, the β-$NaYF_4$:Gd,Yb,Er was about 3–4 nm and RE^{3+} was almost 100% converted. It was worth to notice that α-$NaYF_4$:Gd,Yb,Er was not observed in the experiment, which was different from the previous knowledge of crystal transition from α-phase to β-phase [34]. This should be attributed to the excellent heat transfer ability of the tubular reactor, in which the precursor quickly reached the nucleation temperature of β-phase crystal in contrast to the gradually heating process in batch reactors [35].

Inspired by the continuous synthesis of β-$NaYF_4$:Gd,Yb,Er, we created a two-step strategy for the core–shell UCNPs, as shown in Fig. 3. The first step was to prepare β-$NaYF_4$:Gd,Yb,Er

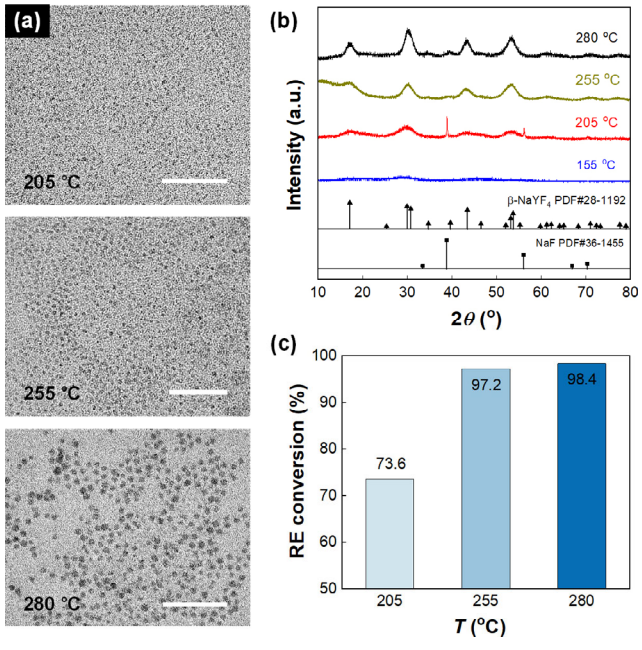

Figure 2 Results of the particle nucleation experiments. (a) Typical TEM images of β-$NaYF_4$:Gd,Yb,Er nuclei from the coiled tube reactor with 8.5 min residence time. Scale bars are 50 nm. (b) XRD patterns of the particles and (c) the RE^{3+} conversions in the tubular reactor at different temperatures. All experiments were carried out at Q = 100 μL·min^{-1}.

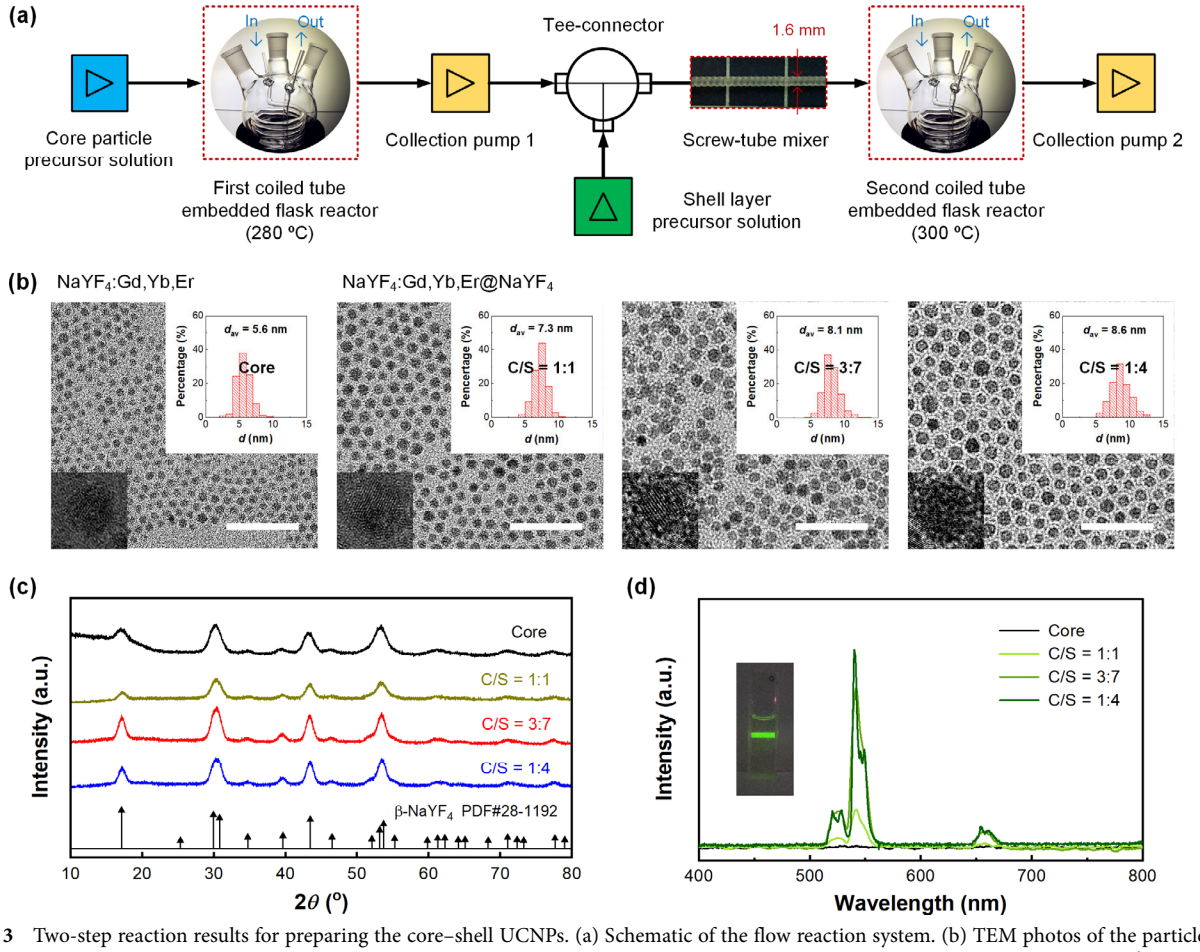

Figure 3 Two-step reaction results for preparing the core–shell UCNPs. (a) Schematic of the flow reaction system. (b) TEM photos of the particles and their diameter statistics. The core particles were from a precursor containing 0.1 M NaOA, 0.16 M NH_4F and 0.04 M $RE(OA)_3$ (50% Y^{3+}, 30% Gd^{3+}, 18% Yb^{3+}, and 2% Er^{3+}) at 100 μL·min^{-1} flow rate. The shells were from a precursor containing 0.1 M NaOA, 0.16 M NH_4F and 0.04 M $Y(OA)_3$ with 100 μL·min^{-1} total flow rate of the core and shell precursor solutions. Core–shell substance ratio (C/S) was equal to the flow rate ratio of the core solution and the shell precursor solution. Scale bars show 50 nm. (c) XRD patterns of the core and core–shell particles. (d) Luminescent spectra of 1 mg·mL^{-1} β-$NaYF_4$:Gd,Yb,Er@$NaYF_4$ cyclohexane solutions excited by a 2 W 980 nm NIR light. The photo shows the particles from the experiment with C/S = 1:4.

cores at 280 °C. After collecting the core particle solution, we directly fed the solution to the second tubular reactor by the first collecting pump. Between the pump and the reactor, a Tee-connector with a home-made screw tube mixer [36] was employed to mix the core solution and the shell processor solution containing 0.1 M NaOA, 0.16 M NH_4F, and 0.04 M $Y(OA)_3$. Because the precursor of the shell did not contain Gd^{3+}, the second reactor was set to 300 °C to accelerate the reaction. β-$NaYF_4$:Gd,Yb,Er@$NaYF_4$ was successfully prepared as shown in Fig. 3(b). Different C/S were studied, and lower C/S resulted to larger core–shell particles. Due to the same hexagonal phase and lattice compatibility of the core and the core–shell particles, TEM images did not show obvious their core–shell structures [9, 37–39]. To demonstrate the core–shell structure of particles, X-ray photoelectron spectroscopy (XPS) analysis was carried out to investigate the surface elements on the particles. According Table 1, the molar ratio of Y/Gd in the core–shell particle surface turned from 10.6 to 41.3, which was much larger than the value of 2.9 in the core particle surface, indicating that the shells were mainly composed by β-$NaYF_4$. The high-resolution transmission electron microscopy (HRTEM) photos in Fig. 3(b) and the XRD spectra in Fig. 3(c) also exhibit the combinations of cores and shells. The luminescence of particles was also evaluated by an exciting experiment with 980 nm NIR light. Figure 3(d) shows the strong green light excited from the β-$NaYF_4$:Gd,Yb,Er@$NaYF_4$ particles. The luminescence of the core–shell particles was over 40 times higher than that of the core particles according to the exciting spectra in the figure.

In addition, the above method was also able to prepare other UCNPs with different colors. Using the precursor solutions with Ho^{3+} and Tm^{3+} as the active elements, we synthesized β-$NaYF_4$:Gd,Yb,Ho@$NaYF_4$ and β-$NaYF_4$:Gd,Yb,Tm@$NaYF_4$ nanoparticles. Without optimizing the reaction conditions, UCNPs emitting yellow and purple luminescence were successfully prepared as shown in Fig. 4. The TEM images and particle diameter distributions show similar sizes of β-$NaYF_4$:Gd,Yb,Ho@$NaYF_4$ and β-$NaYF_4$:Gd,Yb,Tm@$NaYF_4$. Although the particle luminescence was not fully optimized in those experiment, visible yellow and purple lights in Fig. 4 have exhibited the core–shell structures of the UCNPs, since the lights from the core particles were almost invisible under a 2 W laser power.

Table 1 Element content on the particle surfaces from XPS analysis.

Surface elements	Core particle contents (%)	Core–shell particle contents (%)		
		C/S = 1:1	C/S = 3:7	C/S = 1:4
Na	8.35%	7.47%	9.42%	9.64%
F	33.1%	34.6%	41.3%	42.2%
Y	4.31%	7.23%	8.25%	9.50%
Gd	1.45%	0.68%	0.37%	0.23%
C	52.8%	50.0%	40.7%	38.4%

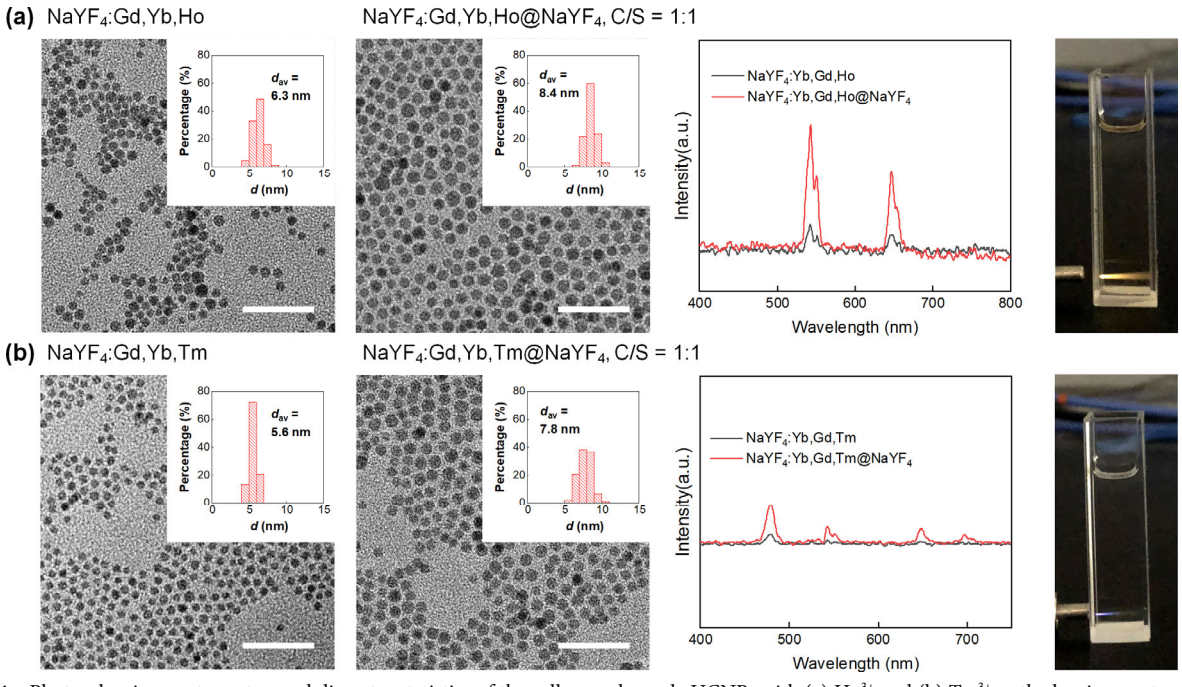

Figure 4 Photos, luminescent spectra, and diameter statistics of the yellow and purple UCNPs with (a) Ho^{3+} and (b) Tm^{3+} as the luminescent sensitizers in the particles. Experiments for the core particles were carried out by using core precursor solutions containing 0.1 M NaOA, 0.16 M NH_4F, and 0.04 M $RE(OA)_3$ (50% Y^{3+}, 30% Gd^{3+}, 18% Yb^{3+}, and 2% Ho^{3+}/Tm^{3+}) and 100 μL·min^{-1} flow rate. Experiments for the shells were carried out by using a shell precursor solution containing 0.1 M NaOA, 0.16 M NH_4F, and 0.04 M $Y(OA)_3$ with 100 μL·min^{-1} total flow rate and 1:1 C/S ratio. Scale bars show 50 nm. 1 mg·mL^{-1} core–shell particle cyclohexane solutions excited by the 980 nm NIR light show visible luminescent lights

3 Conclusions

In summary, we proposed a flow chemistry method for the solvothermal co-precipitation reaction to synthesize ultrasmall core–shell UCNPs. Coiled tube embedded flask reactors that can provide stable reaction temperature were developed for the up to 300 °C reaction, where the particles quickly nucleated in less than 9 min. A two-step reaction strategy without intermediate purification was created based on the coiled tubular reactor, and β-$NaYF_4$:Gd,Yb,Er/Ho/Tm@$NaYF_4$ below 10 nm but with strong luminescence ability were successfully prepared as a prototype for preparing UCNPs with high efficiency.

4 Methods

4.1 Sources of chemicals

Yttrium acetate hydrate (99.99%), ytterbium acetate hydrate (99.99%), gadolinium acetate hydrate (99.99%), erbium acetate hydrate (99.9%), holmium acetate hydrate (99.9%), and thulium acetate hydrate (99.9%) were from Shandong DESHENG New Material Co., Ltd. Ammonium fluoride (analytical reagent (AR)) was from Tianjin FUCHEN Chemical Reagent Factory. Oleic acid (90%) and 1-octadecene (90%) were from Alfa Aesar USA. Sodium hydroxide (AR) was from Beijing TONGGUANG Fine Chemicals. Cyclohexane (AR) was from Beijing BEIHUA Fine Chemicals Co., Ltd. Methanol (AR) was from Shanghai TITAN Scientific Co., Ltd. All chemicals were used without purification.

4.2 Preparation of the rare earth oleate $RE(OA)_3$ solution

$RE(OA)_3$ was made from the rare earth acetate hydrate in the mixture of HOA and ODE. In this process, 4.0 mmol $RE(Ac)_3$ (50%Y, 30%Gd, 18%Yb, 2%Er/Tm/Ho in molar percentage for the cores) or 4.0 mmol $Y(Ac)_3$ (for the shell), 40 mL HOA, and 60 mL ODE were loaded in a 250 mL three-necked bottle at first. The mixture was then heated to 150 °C and maintained for 30 min under the protection of argon to vaporize the acetic acid, which resulted to a transparent solution. The $RE(OA)_3$ solution was then used to prepare the precursor solution of the UCNPs.

4.3 Preparation of the precursor solutions

2.5 mL 1 M NaOH methanol solution was added into 25 mL $RE(OA)_3$ solution at 45 °C. Then, the mixture was heated to 130 °C under the protection of argon and stirred for 30 min to make NaOH and HOA fully convert to NaOA. Subsequently, the mixture was cooled down to 45 °C and blended with 8 mL 0.5 M NH_4F methanol solution. The mixture was further stirred for 30 min at 45 °C and then heated up to 100 °C to evaporate the methanol and water under vacuum. The obtained precursor solution was named as PS–Y, PS–Y:Gd,Yb,Er, PS–Y:Gd,Yb,Tm, and PS–Y:Gd,Yb,Ho corresponding to the RE composition.

4.4 Experiment of β-$NaREF_4$ core particle synthesis

To synthesize β-$NaYF_4$:Gd,Yb,Er, the precursor solutions PS–Y:Gd,Yb,Er with 0.02–0.08 mol·L^{-1} RE^{3+} were pressed through the flask reactor employing 3.7 mm inner-diameter and 6 mm out-diameter tube with flow rates of 50, 100 and 150 μL·min^{-1}. The reaction temperature was controlled from 260 to 300 °C. The product solution was collected at the outlet of the reactor, which had been cooling down to 25 °C room temperature, by a syringe pump with a 25 mL glass syringe. The product solution was then mixed with equal volume of ethanol after collection to precipitate the particles, which were subsequently centrifugally separated for at least 10 min. After the separation, the mother liquor was restored to determine the concentration of resident RE^{3+}. The solids were double washed by cyclohexane and finally dispersed into cyclohexane for further characterization. The syntheses of β-$NaYF_4$:Gd,Yb,Tm and β-$NaYF_4$:Gd,Yb,Ho from PS–Y:Gd,Yb,Tm and PS–Y:Gd,Yb,Ho were the same as those for β-$NaYF_4$:Gd,Yb,Er nanoparticles.

4.5 Experiment of the nucleation of β-$NaREF_4$ particles

To study the particle nucleation in the tubular flow reactor, β-$NaYF_4$:Gd,Yb,Er was selected for a test. The precursor solution PS–Y:Gd,Yb,Er with 0.04 M RE^{3+} was continuously injected into the 1 mm inner-dameter and 3 mm out-diameter quartz reactor, temperature of which was controlled from 205 to 280 °C. The flow rate was at 100 μL·min^{-1}, which resulted in a residence time of 8–9 minutes. The methods of collection and purification of product particles were the same as above.

4.6 Experiment of β-$NaREF_4$@β-$NaYF_4$ particle synthesis

To synthesize the core particles, the precursor solutions PS–Y:Gd,Yb,Er, PS–Y:Gd,Yb,Tm, and PS–Y:Gd,Yb,Ho with 0.04 M RE^{3+} were pressed through the first flask reactor employing 3.7 mm inner-diameter tube at a flow rate of 100 μL·min^{-1}. The reaction temperature was controlled at 280 °C. To synthesize the shells, the precursor solution PS–Y with 0.04 M Y^{3+} was mixed with the core particle solution in the screw-tube mixer at a total flow rate of 100 μL·min^{-1}. The core–shell substance ratio varied from 1:1 to 1:4 in the experiment via varying the flow rate ratio of the core particle solution and the shell precursor solution. The reaction temperature in the second flask reactor was set to 300 °C. The product solution was finally collected by a syringe pump with a 25 mL glass syringe. The purification step was the same as those shown in Section 4.4.

4.7 Determination of the RE^{3+} concentration in the product solution

10 mL 2.0 M HCl aqueous solution and 10 mL mother liquor from the centrifugal separation were mixed in a sampling bottle. To extract the rare-earth ions from the mother liquor to the HCl solution, the mixture was stored in a shaker (HZ-9212S, Taicang Science and Education Instrument, China) worked at 200 rpm frequency for 4 h at 25 °C. After 1 h of phase separation, the RE^{3+} concentration in the aqueous phase was titrated against ethylene diamine tetraacetic acid (EDTA). Finally, RE^{3+} concentration in the production solution was calculated from mass balance, and the conversion of RE^{3+} was obtained from the concentration difference in the original and production solutions.

4.8 Material characterization methods

The particles were determined from TEM (HITACHI, HT-7700) images. At least 300 particles of each sample were counted for the average diameters and standard deviations. HRTEM photographs were obtained from a JEOL TEM (JEM–2100F, at 200 kV). The particle crystal form was analyzed by XRD using an X-ray diffractometer (Bruker, D8 Advance) with Cu Kα radiation. Particle surface element was determined by an XPS spectrometer (ESCALAB 250XI, Thermo Fisher Scientific) with Al target as the X-ray source. UV–vis spectrometer (USB 2000+, Ocean Optics) was used to determine the upconversion luminescent spectroscopies of the particles in cyclohexane (1 mg·mL^{-1}) with an infrared diode laser (MLL-Ⅲ-980, Changchun New Industry Optoelectronics Technology) as the light source, which had an excitation power of 2 W.

Acknowledgements

The authors acknowledge the supports from the National Natural Science Foundation of China (Nos. 21991104 and 92034303).

Electronic Supplementary Material: Supplementary material (details of reaction platform and some additional experimental results, which include the influences of flow rate and precursor concentration on the generation of β-$NaREF_4$, surface elemental analysis for the core and core–shell particles by XPS and TEM, as well as CFD simulation methods and results) is available in the online version of this article at https://doi.org/10.1007/s12274-021-3625-3.

References

[1] Chen, G. Y.; Ågren, H.; Ohulchanskyy, T. Y.; Prasad, P. N. Light upconverting core–shell nanostructures: Nanophotonic control for emerging applications. *Chem. Soc. Rev.* **2015**, *44*, 1680–1713.

[2] Chen, G. Y.; Qiu, H. L.; Prasad, P. N.; Chen, X. Y. Upconversion nanoparticles: Design, nanochemistry, and applications in theranostics. *Chem. Rev.* **2014**, *114*, 5161–5214.

[3] Park, Y. I.; Lee, K. T.; Suh, Y. D.; Hyeon, T. Upconverting nanoparticles: A versatile platform for wide-field two-photon microscopy and multi-modal *in vivo* imaging. *Chem. Soc. Rev.* **2015**, *44*, 1302–1317.

[4] Liu, Q.; Sun, Y.; Yang, T. S.; Feng, W.; Li, C. G.; Li, F. Y. Sub-10 nm hexagonal lanthanide-doped $NaLuF_4$ upconversion nanocrystals for sensitive bioimaging *in vivo*. *J. Am. Chem. Soc.* **2011**, *133*, 17122–17125.

[5] Kobayashi, H.; Ogawa, M.; Alford, R.; Choyke, P. L.; Urano, Y. New strategies for fluorescent probe design in medical diagnostic imaging. *Chem. Rev.* **2010**, *110*, 2620–2640.

[6] Xu, J. T.; Han, W.; Yang, P. P.; Jia, T.; Dong, S. M.; Bi, H. T.; Gulzar, A.; Yang, D.; Gai, S. L.; He, F. et al. Tumor microenvironment-responsive mesoporous MnO_2-coated upconversion nanoplatform for self-enhanced tumor theranostics. *Adv. Fucnt. Mater.* **2018**, *28*, 1803804.

[7] Liu, Y. Y.; Meng, X. F.; Bu, W. B. Upconversion-based photodynamic cancer therapy. *Coordin. Chem. Rev.* **2019**, *379*, 82–98.

[8] Zhang, Y.; Yu, Z. Z.; Li, J. Q.; Ao, Y. X.; Xue, J. W.; Zeng, Z. P.; Yang, X. L.; Tan, T. T. Y. Ultrasmall-superbright neodymium-upconversion nanoparticles via energy migration manipulation and lattice modification: 808 nm-activated drug release. *ACS Nano* **2017**, *11*, 2846–2857.

[9] Chen, G. Y.; Ohulchanskyy, T. Y.; Kumar, R.; Ågren, H.; Prasad, P. N. Ultrasmall monodisperse $NaYF_4$:Yb^{3+}/Tm^{3+} nanocrystals with enhanced near-infrared to near-infrared upconversion photoluminescence. *ACS Nano* **2010**, *4*, 3163–3168.

[10] Wang, F.; Wang, J.; Liu, X. G. Direct evidence of a surface quenching effect on size-dependent luminescence of upconversion nanoparticles. *Angew. Chem., Int. Ed.* **2010**, *49*, 7456–7460.

[11] Würth, C.; Fischer, S.; Grauel, B.; Alivisatos, A. P.; Resch-Genger, U. Quantum yields, surface quenching, and passivation efficiency for ultrasmall core/shell upconverting nanoparticles. *J. Am. Chem. Soc.* **2018**, *140*, 4922–4928.

[12] Quintanilla, M.; Ren, F. Q.; Ma, D. L.; Vetrone, F. Light management in upconverting nanoparticles: Ultrasmall core/shell architectures to tune the emission color. *ACS Photonics* **2014**, *1*, 662–669.

[13] Xue, M.; Zhu, X. J.; Qiu, X. C.; Gu, Y. Y.; Feng, W.; Li, F. Y. Highly enhanced cooperative upconversion luminescence through energy transfer optimization and quenching protection. *ACS Appl. Mater. Interfaces* **2016**, *8*, 17894–17901.

[14] Dühnen, S.; Rinkel, T.; Haase, M. Size control of nearly monodisperse β-$NaGdF_4$ particles prepared from small α-$NaGdF_4$ nanocrystals. *Chem. Mater.* **2015**, *27*, 4033–4039.

[15] Fischer, S.; Swabeck, J. K.; Alivisatos, A. P. Controlled isotropic and anisotropic shell growth in β-$NaLnF_4$ nanocrystals induced by precursor injection rate. *J. Am. Chem. Soc.* **2017**, *139*, 12325–12332.

[16] Zeng, J. H.; Su, J.; Li, Z. H.; Yan, R. X.; Li, Y. D. Synthesis and upconversion luminescence of hexagonal-phase $NaYF_4$:Yb, Er^{3+} phosphors of controlled size and morphology. *Adv. Mater.* **2005**, *17*, 2119–2123.

[17] Shi, R. K.; Ling, X. C.; Li, X. N.; Zhang, L.; Lu, M.; Xie, X. J.; Huang, L.; Huang, W. Tuning hexagonal $NaYbF_4$ nanocrystals

down to sub-10 nm for enhanced photon upconversion. *Nanoscale* **2017**, *9*, 13739–13746.

[18] Rinkel, T.; Raj, A. N.; Dühnen, S.; Haase, M. Synthesis of 10 nm β-$NaYF_4$:Yb,Er/$NaYF_4$ core/shell upconversion nanocrystals with 5 nm particle cores. *Angew. Chem., Int. Ed.* **2016**, *55*, 1164–1167.

[19] Pu, Y.; Leng, J. N.; Wang, D.; Wang, J. X.; Foster, N. R.; Chen, J. F. Process intensification for scalable synthesis of ytterbium and erbium co-doped sodium yttrium fluoride upconversion nanodispersions. *Powder Technol.* **2018**, 340, 208–216.

[20] Jiao, Y. R.; Pu, Y.; Wang, J. X.; Wang, D.; Chen, J. F. Process intensified synthesis of rare-earth doped β-$NaYF_4$ nanorods toward gram-scale production. *Ind. Eng. Chem. Res.* **2019**, 58, 22306–22314.

[21] Tofighi, G.; Gaur, A.; Doronkin, D. E.; Lichtenberg, H.; Wang, W.; Wang, D.; Rinke, G.; Ewinger, A.; Dittmeyer, R.; Grunwaldt, J. D. Microfluidic synthesis of ultrasmall AuPd nanoparticles with a homogeneously mixed alloy structure in fast continuous flow for catalytic applications. *J. Phys. Chem. C* **2018**, *122*, 1721–1731.

[22] Frenz, L.; El Harrak, A.; Pauly, M.; Bégin-Colin, S.; Griffiths, A. D.; Baret, J. C. Droplet-based microreactors for the synthesis of magnetic iron oxide nanoparticles. *Angew. Chem., Int. Ed.* **2008**, *47*, 6817–6820.

[23] Kumar, K.; Nightingale, A. M.; Krishnadasan, S. H.; Kamaly, N.; Wylenzinska-Arridge, M.; Zeissler, K.; Branford, W. R.; Ware, E.; deMello, A. J.; deMello, J. C. Direct synthesis of dextran-coated superparamagnetic iron oxide nanoparticles in a capillary-based droplet reactor. *J. Mater. Chem.* **2012**, *22*, 4704–4708.

[24] Hung, L. H.; Choi, K. M.; Tseng, W. Y.; Tan, Y. C.; Shea, K. J.; Lee, A. P. Alternating droplet generation and controlled dynamic droplet fusion in microfluidic device for CdS nanoparticle synthesis. *Lab Chip* **2006**, *6*, 174–178.

[25] Baek, J.; Shen, Y.; Lignos, I.; Bawendi, M. G.; Jensen, K. F. Multistage microfluidic platform for the continuous synthesis of III-V core/shell quantum dots. *Angew. Chem., Int. Ed.* **2018**, *57*, 10915–10918.

[26] Abdel-Latif, K.; Bateni, F.; Crouse, S.; Abolhasani, M. Flow synthesis of metal halide perovskite quantum dots: From rapid parameter space mapping to AI-guided modular manufacturing. *Matter* **2020**, *3*, 1053–1086.

[27] Abdel-Latif, K.; Epps, R. W.; Kerr, C. B.; Papa, C. M.; Castellano, F. N.; Abolhasani, M. Facile room-temperature anion exchange reactions of inorganic perovskite quantum dots enabled by a modular microfluidic platform. *Adv. Funct. Mater.* **2019**, 29, 1900712.

[28] Liu, Z. D.; Wakihara, T.; Nishioka, D.; Oshima, K.; Takewaki, T.; Okubo, T. One-minute synthesis of crystalline microporous aluminophosphate ($AlPO_4$-5) by combining fast heating with a seed-assisted method. *Chem. Commun.* **2014**, 50, 2526–2528.

[29] Zhang, Y. H.; Huang, L.; Liu, X. G. Unraveling epitaxial habits in the $NaLnF_4$ system for color multiplexing at the single-particle level. *Angew. Chem., Int. Ed.* **2016**, *128*, 5812–5816.

[30] Zhang, C.; Lee, J. Y. Prevalence of anisotropic shell growth in rare earth core–shell upconversion nanocrystals. *ACS Nano* **2013**, *7*, 4393–4402.

[31] Wang, F.; Deng, R. R.; Liu, X. G. Preparation of core-shell $NaGdF_4$ nanoparticles doped with luminescent lanthanide ions to be used as upconversion-based probes. *Nat. Protoc.* **2014**, *9*, 1634–1644.

[32] Wang, F.; Han, Y.; Lim, C. S.; Lu, Y. H.; Wang, J.; Xu, J.; Chen, H. Y.; Zhang, C.; Hong, M. H.; Liu, X. G. Simultaneous phase and size control of upconversion nanocrystals through lanthanide doping. *Nature* **2010**, *463*, 1061–1065.

[33] Shi, F.; Zhao, Y. Sub-10 nm and monodisperse β-$NaYF_4$:Yb,Tm,Gd nanocrystals with intense ultraviolet upconversion luminescence. *J. Mater. Chem. C.* **2014**, *2*, 2198–2203.

[34] Wang, J.; Song, H. W.; Xu, W.; Dong, B.; Xu, S.; Chen, B. T.; Yu, W.; Zhang, S. Phase transition, size control and color tuning of $NaREF_4$:Yb^{3+}, Er^{3+} (RE = Y, Lu) nanocrystals. *Nanoscale* **2013**, *5*, 3412–3420.

[35] Homann, C.; Krukewitt, L.; Frenzel, F.; Grauel, B.; Würth, C.; Resch-Genger, U.; Haase, M. $NaYF_4$:Yb,Er/$NaYF_4$ core/shell nanocrystals with high upconversion luminescence quantum yield. *Angew. Chem., Int. Ed.* **2018**, *57*, 8765–8769.

[36] Wang, K.; Zhang, H. M.; Shen, Y.; Adamo, A.; Jensen, K. F. Thermoformed fluoropolymer tubing for in-line mixing. *React. Chem. Eng.* **2018**, *3*, 707–713.

[37] Pilch, A.; Würth, C.; Kaiser, M.; Wawrzyńczyk, D.; Kurnatowska, M.; Arabasz, S.; Prorok, K.; Samoć, M.; Strek, W.; Resch-Genger, U. et al. Shaping luminescent properties of Yb^{3+} and Ho^{3+} Co-doped upconverting core-shell β-$NaYF_4$ nanoparticles by dopant distribution and spacing. *Small* **2017**, *13*, 1701635.

[38] Mai, H. X.; Zhang, Y. W.; Sun, L. D.; Yan, C. H. Highly efficient multicolor up-conversion emissions and their mechanisms of monodisperse $NaYF_4$:Yb,Er core and core/shell-structured nanocrystals. *J. Phys. Chem. C* **2007**, *111*, 13721–13729.

[39] Boyer, J. C.; Gagnon, J.; Cuccia, L. A.; Capobianco, J. A. Synthesis, characterization, and spectroscopy of $NaGdF_4$: Ce^{3+},Tb^{3+}/$NaYF_4$ core/shell nanoparticles. *Chem. Mater.* **2007**, *19*, 3358–3360.